J Eng Math (2015) 95:101–119
DOI 10.1007/s10665-014-9728-z

Area-preserving azimuthal shear deformation of an incompressible tube reinforced by radial fibres

M. A. Dagher · K. P. Soldatos

Received: 21 February 2014 / Accepted: 19 July 2014 / Published online: 8 November 2014

Abstract The principal problem of interest in this paper is that of the area-preserving azimuthal shear strain of an incompressible transversely isotropic hyper-elastic circular cylindrical tube subjected to homogeneous radial tractions on both its inner and outer boundaries. A considerable part of the solution to this problem is achieved numerically. A comparison is made between the stress distributions obtained here when fibres are very strong and their counterparts obtained in the limiting case of an ideal fibre-reinforced material [Soldatos, J Eng Math 68(1):99–127, 2010]. Pure azimuthal shear strain may be considered as a particular case of the present deformation. However, in the present case, equilibrium requires a change of the inner and outer tube boundaries which, due to the incompressibility constraint, may take place only in a manner which preserves the area of the tube cross section. Another particular case is the isotropic material counterpart of the present problem, which was considered previously [Dagher and Soldatos, J Eng Math 78(1):131–142, 2013].

Keywords Azimuthal shear strain · Finite strain · Hyper-elasticity · Incompressibility · Reinforced neo-Hookean material · Transverse isotropy

1 Introduction

The classic version of the problem of azimuthal shear deformation of an elastic circular cylindrical tube of infinite extent is due to [1] and, in several forms and variations, has been considered and studied since then by several investigators. This refers to a particular, plane-strain type of finite strain that is applied on the cross section of an incompressible isotropic hyper-elastic circular cylindrical tube. Accordingly, under the action of an appropriate set of boundary conditions, the tube cross section is subjected to pure azimuthal shear strain during which it remains

M. A. Dagher · K. P. Soldatos (✉)
School of Mathematical Sciences, University of Nottingham, Nottingham NG9 3LF, UK
e-mail: Kostas.Soldatos@nottingham.ac.uk

K. P. Soldatos
Spencer Institute of Theoretical and Computational Mechanics, University of Nottingham, Nottingham, UK

M. A. Dagher
Department of Science and Engineering Mathematics, Faculty of Petroleum and Mining Engineering, Suez University, Suez, Egypt

circular while its inner and outer radii do not change. While most relevant studies refer to the case in which the tube hyper-elastic material is isotropic, [2] introduced a new version of the problem in which the tube cross section is reinforced by a single family of unidirectional extensible fibres. A second family of plane extensible fibres was more recently placed also on the tube cross section [3], thereby assuming that anisotropy proceeds beyond the relatively simple symmetries of the transverse isotropy assumed in [2].

Another relevant problem [4,5] deals with the azimuthal shear strain of an incompressible hyper-elastic circular cylindrical tube having its cross section reinforced by a single family of inextensible fibres. This new development [4,5] made it clear that pure azimuthal shear strain is not possible when the incompressible material of the tube contains an inextensible direction of transverse isotropy. Unlike [2] or [3], where extension or contraction of fibres is assumed possible, a single family of inextensible fibres causes a change in both the inner and outer tube radii in a manner that preserves the area of the tube cross section. Recall that in this context an incompressible material which is further reinforced by one or more families of inextensible fibres is known as ideal fibre-reinforced material [6]. In addition, when attainable, pure azimuthal shear strain [1–3] is essentially a particular case of the more general *area-preserving* type of azimuthal shear strain considered in [4,5].

Area-preserving azimuthal shear deformation was considered in [4,5] as an application of a study having as its principal purpose to investigate the influence that certain second-gradient effects related to fibre-bending stiffness exert on finite plane deformations of ideal fibre-reinforced hyper-elastic solids. However, this type of deformation was found to be attainable by an ideal fibre-reinforced tube regardless of whether the inextensible fibres involved possess bending stiffness or are, instead, perfectly flexible. Moreover, [4,5] revealed that, if those inextensible fibres are initially straight and aligned along the radial direction of the tube cross section, then they remain straight during deformation and force the tube to undergo area-preserving azimuthal shear strain by changing their slope only. It was thus concluded [4,5] that if the direction of transverse isotropy is due to the existence of strong, nearly inextensible fibres, then the tube should be expected to resist considerably the conditions of pure azimuthal shear deformation assumed in [1–3]. In that case, some tendency should instead be observed towards creating a deformation pattern that couples azimuthal shear strain with radial stretching.

In this context, the ideal fibre-reinforced material concept employed in [4,5] leads to a first approximation solution of the finite azimuthal shear strain problem of a cylindrical tube reinforced by radial fibres. It is noted in this connection that the principal problem encountered in nature is that of a relevant transversely isotropic tube made of completely unconstrained material. However, many materials are nearly incompressible, and, similarly, many kinds of natural or structural fibres are or, under certain circumstances, behave as nearly inextensible. Thus, in many cases of interest, the corresponding problem of extensible fibres embedded in an incompressible material [2] or that of a compressible material reinforced by inextensible fibres serves as a realistic and plausible simplification of the aforementioned principal problem. Either of these simplified problems is regarded as an intermediate step between the completely unconstrained problem and its doubly constrained version considered in [4,5]. Further progress in the subject may, therefore, become possible by dismissing one or both of the material constraints involved in [4,5].

Under these considerations, this investigation dismisses the constraint of fibre inextensibility and deals with the problem of the area-preserving azimuthal shear strain of an incompressible tube reinforced by a single family of straight, extensible and perfectly flexible fibres aligned along the radial direction of the tube cross section. The corresponding problem of pure azimuthal shear strain was already considered in [2] as a particular case of a more general fibre configuration, while here it is regarded as a particular case of the assumed more general deformation pattern. Finally, it is of interest to note that, in the absence of fibres, the present formulation and its associated solution reduce naturally to their counterparts detailed in [7] for the problem of area-preserving azimuthal shear deformation of an incompressible hyper-elastic isotropic tube.

The article is organised as follows. Section 2 provides a complete description of the present problem of interest, and Sect. 3 outlines its solution for a general form of the strain energy density. A detailed form of that solution is then presented in Sect. 4 for a particular case in which the strain energy density is that of the reinforced neo-Hookean material [8]. The corresponding solution, which is based on the concept of ideal fibre-reinforced materials [4], is then presented in Sect. 5 for numerical comparison purposes, with the help of an appendix. Thus, the numerical results presented in Sect. 6 illustrate that the new hyper-elasticity solution detailed in Sects. 3 and 4 is essentially

an intermediate step between the isotropic material solution obtained in [7] and that of the ideal fibre-reinforced material obtained in [4,5]. Section 7 summarises the main conclusions of this study.

2 Problem formulation

In its undeformed configuration, which is assumed to be unstressed, the geometry of a circular cylindrical tube of infinite extent is defined as follows:

$$B_0 \le R \le B_1, \qquad 0 \le \Theta \le 2\pi, \qquad -\infty \le Z \le \infty. \tag{2.1}$$

Here, R, Θ and Z are appropriate cylindrical polar co-ordinate parameters in the reference configuration, and the non-negative constants B_0 and B_1 represent the inner and outer radii of the tube respectively; $B_0 = 0$ is the case of a non-hollow (solid) cylinder. The axially symmetric azimuthal shear deformation of interest is described as follows:

$$r = r(R), \qquad \theta = \Theta + g(R), \qquad z = Z, \tag{2.2}$$

where r, θ and z represent cylindrical polar co-ordinate parameters in the deformed configuration. Both functions $r(R)$ and $g(R) = \hat{g}(r)$ are to be determined.

The deformation gradient and the left Cauchy–Green deformation tensors are respectively

$$\begin{aligned}
\mathbf{F} &= \begin{pmatrix} \dfrac{\partial r}{\partial R} & \dfrac{1}{R}\dfrac{\partial r}{\partial \Theta} & \dfrac{\partial r}{\partial Z} \\ r\dfrac{\partial \theta}{\partial R} & \dfrac{r}{R}\dfrac{\partial \theta}{\partial \Theta} & r\dfrac{\partial \theta}{\partial Z} \\ \dfrac{\partial z}{\partial R} & \dfrac{1}{R}\dfrac{\partial z}{\partial \Theta} & \dfrac{\partial z}{\partial Z} \end{pmatrix} = \begin{pmatrix} r'(R) & 0 & 0 \\ rg'(R) & r/R & 0 \\ 0 & 0 & 1 \end{pmatrix} = \begin{pmatrix} r'(R) & 0 & 0 \\ \gamma & \chi^{-1} & 0 \\ 0 & 0 & 1 \end{pmatrix}, \\
\mathbf{B} &= \mathbf{F}\mathbf{F}^{\mathrm{T}} = \begin{pmatrix} r'^2(R) & rr'(R)g'(R) & 0 \\ rr'(R)g'(R) & r^2 g'^2(R) + r^2/R^2 & 0 \\ 0 & 0 & 1 \end{pmatrix} = \begin{pmatrix} r'^2(R) & \gamma r'(R) & 0 \\ \gamma r'(R) & \gamma^2 + \chi^{-2} & 0 \\ 0 & 0 & 1 \end{pmatrix}
\end{aligned} \tag{2.3}$$

and make evident the plane-strain nature of the deformation (2.2). Here, as well as in what follows, a prime denotes differentiation of a function with respect to its argument and superscript T indicates the transpose of a matrix. Moreover,

$$\chi = \frac{R}{r} \qquad \text{and} \qquad \gamma = rg'(R) = R\hat{g}'(r) \tag{2.4}$$

are respectively the radial stretch and the amount of shear involved in the deformation.

It is now assumed that the tube material is incompressible and, hence, the material incompressibility constraint, $\det(\mathbf{F}) = 1$, requires that $rr'/R = 1$. The solution of this first-order ordinary differential equation yields

$$r(R) = \sqrt{R^2 + c} \quad (c \ge -B_0^2), \tag{2.5}$$

where c is an arbitrary constant of integration with dimensions of area. Based on purely geometrical considerations, the restriction $c \ge -B_0^2$ should be imposed on c. This is the principal parameter that characterises the assumed deformation and must be determined; here, equality is possible only if the assumed deformation can convert the tube into a non-hollow (solid) cylinder.

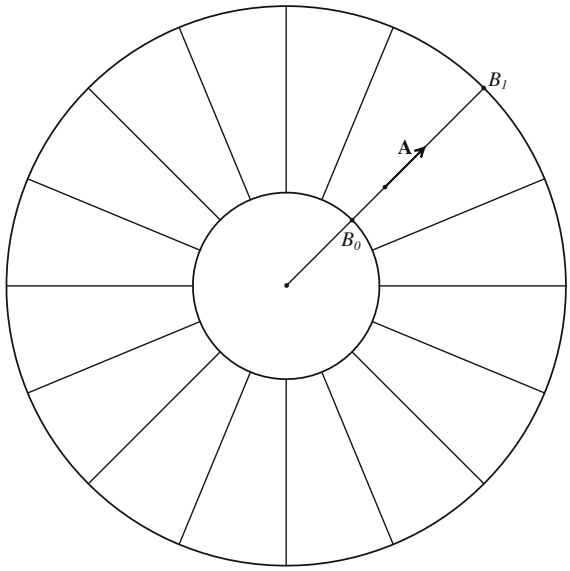

Fig. 1 Undeformed tube cross section reinforced by straight radial fibres

Pure azimuthal shear deformation is obtained as a particular case of the outlined deformation by setting $c = 0$ in (2.5). In that case, the inner and outer radii of the tube remain unchanged after deformation, provided that some specific set of non-zero radial traction is assigned on the tube boundaries [1]. If, on the other hand, $c > 0$ ($c < 0$), then the inner and outer tube radii expand (contract) simultaneously and become

$$\hat{b}_n = \sqrt{B_n^2 + c} \qquad (n = 0, 1). \tag{2.6}$$

A direction of transverse isotropy is now introduced on the plane of the undeformed tube cross section caused by the existence of a single family of plane fibres aligned along its radial direction. The unit tangent of that family of plane material curves (Fig. 1) is

$$\mathbf{A} = (A_R, A_\Theta, A_Z)^{\mathrm{T}}, \qquad A_R = 1, \qquad A_\Theta = 0, \qquad A_Z = 0. \tag{2.7}$$

After deformation, the new direction of the fibres is defined by the vector

$$\mathbf{b} = \mathbf{F}\mathbf{A}, \tag{2.8}$$

with components

$$b_r = \chi, \qquad b_\theta = \gamma, \qquad b_z = 0. \tag{2.9}$$

For the hyper-elasticity plane-strain problem of interest, material constitution should comply with the fact that the strain energy density, W, is a function of at most two independent invariants (e.g. [9]), namely

$$W = W(J_1, J_2), \qquad J_1 = \mathrm{tr}(\mathbf{B}), \qquad J_2 = \mathbf{b}^{\mathrm{T}}\mathbf{b}. \tag{2.10}$$

Thus, the constitutive equation of the material may be expressed as follows (see also [2]):

$$\mathbf{t} = -p\mathbf{I} + 2W_1\mathbf{B} + 2W_2\mathbf{b} \otimes \mathbf{b}, \tag{2.11}$$

where $\mathbf{t}$ is the Cauchy stress tensor, $\mathbf{I}$ is the identity tensor, p is the arbitrary hydrostatic pressure which represents the reaction of the material to the incompressibility constraint and $W_i = \partial W/\partial J_i$ $(i = 1, 2)$.

Using (2.3b) and (2.9), it is seen that

$$J_1 = \chi^2 + \gamma^2 + \chi^{-2} + 1, \qquad J_2 = \chi^2 + \gamma^2, \tag{2.12}$$

and, hence, (2.11) yields explicitly the in-plane stress components as follows:

$$\begin{aligned} t_{rr} &= -p + 2W_1\chi^2 + 2W_2\chi^2, \\ t_{\theta\theta} &= -p + 2W_1(\gamma^2 + \chi^{-2}) + 2W_2\gamma^2, \\ t_{r\theta} &= 2W_1\gamma\chi + 2W_2\chi\gamma. \end{aligned} \tag{2.13}$$

It is convenient to note for later use that, in the light of (2.10) and (2.12), the strain energy density can alternatively be expressed in the form

$$W = \tilde{W}(\gamma, \chi), \tag{2.14}$$

and, hence, using (2.13c), to yield

$$t_{r\theta} = \chi \tilde{W}_\gamma, \tag{2.15}$$

where $\tilde{W}_\gamma = \partial \tilde{W}/\partial\gamma$.

In the absence of body forces, equilibrium in the radial and azimuthal directions requires satisfaction respectively of the following equations:

$$\frac{\mathrm{d}t_{rr}}{\mathrm{d}r} = \frac{1}{r}\,(t_{\theta\theta} - t_{rr})\,, \quad \frac{\mathrm{d}}{\mathrm{d}r}\left(r^2 t_{r\theta}\right) = 0. \tag{2.16}$$

Equilibrium along the axial tube direction is satisfied by considering p independently of z. In what follows, a solution of this system of equations will be sought for the case where the tube maintains its circular cylindrical shape under the imposed deformation (2.2), subject to a set of appropriate boundary conditions.

Accordingly, the following boundary conditions are imposed at $R = B_0$:

$$t_{rr} = 0, \qquad \theta - \Theta = g(B_0) = 0, \tag{2.17}$$

thereby implying that the inner boundary of the tube cross section is restrained from rotation but its radius is free to expand or contract. On the other hand, the following set of boundary conditions is applied on the outer tube boundary, $R = B_1$:

$$t_{rr} = 0 \quad \text{and either} \quad \theta - \Theta = g(B_1) = \psi \quad \text{or} \quad t_{r\theta}(\hat{b}_1) = \tau_\theta, \tag{2.18}$$

whose radius is therefore also free to expand or contract. It is emphasised that only one of the two constant quantities ψ and τ_θ is considered to be known on the tube outer boundary; the other is to be determined from the solution of the problem. That known quantity is identified as the external cause of the deformation of interest and, if positive (negative), causes anti-clockwise (clockwise) rotation of the outer boundary.

3 Solution procedure

Integrating the azimuthal equilibrium Eq. (2.16b) in association with the boundary condition (2.18c) yields

$$t_{r\theta} = \frac{\tau_\theta \hat{b}_1^2}{r^2}. \tag{3.1}$$

When compared with (2.15), this yields

$$\chi \tilde{W}_\gamma = \frac{\tau_\theta \hat{b}_1^2}{r^2}, \tag{3.2}$$

which, using Eq. (2.4b) and for a given form of $\tilde{W}$, will provide an ordinary differential equation for the unknown deformation function $g(R)$. Appropriate integration of the latter provides $g(R)$, as well as γ, through further use of (2.4b).

Recall that, on the basis of (3.1) and (3.2), with $\chi = 1$, the restriction

$$\gamma \gtreqless 0 \quad \text{as} \quad \tau_\theta \gtreqless 0 \tag{3.3}$$

was imposed in [2] for a solution to the corresponding pure azimuthal shear-strain problem considered and studied there. Because the radial stretching χ is necessarily positive, the physical concepts and the reasoning that underpinned the validity of (3.3) in [2] remain intact in the present case. Hence, (3.3) will remain unchanged in what follows.

Using Eqs. (2.13a,b), it is next seen that

$$t_{\theta\theta} - t_{rr} = \gamma \tilde{W}_\gamma - \chi \tilde{W}_\chi, \tag{3.4}$$

where $\tilde{W}_\chi = \partial \tilde{W}/\partial \chi$. This is inserted into the radial equilibrium Eq. (2.16a), which, in the light of (3.2), is integrated with the simultaneous use of the boundary condition (2.17a) to yield

$$t_{rr} = \int_{\hat{b}_0}^{r} \left(\frac{\tau_\theta \hat{b}_1^2 \gamma}{\chi r^3} - \frac{\chi}{r} \tilde{W}_\chi \right) \mathrm{d}r. \tag{3.5}$$

Association of this result with the boundary condition (2.18a) leads to

$$I(c) \equiv \int_{\hat{b}_0}^{\hat{b}_1} \left(\frac{\tau_\theta \hat{b}_1^2 \gamma}{\chi r^3} - \frac{\chi}{r} \tilde{W}_\chi \right) \mathrm{d}r = 0. \tag{3.6}$$

Equations (2.4) make clear that this is essentially an algebraic equation for the remaining unknown parameter, c.

For any given form of $\tilde{W}$, the function $I(c)$ may be plotted on the cI-plane, where the actual value sought for c is identified as the point of intersection of that plot with the c-axis. The integration involved in (3.6) must be performed numerically, as many times as is necessary, during the outlined c-determination process. The mathematical procedure outlined in this section for the determination of the unknown parameter c, as well as the deformation function $g(R)$ and the associated stress distributions, is employed in the next section for a particular case of the strain energy density.

4 Application: the reinforced neo-Hookean material

For the purpose of an application, consider the strain energy density of the reinforced neo-Hookean material, namely [8]:

$$W(J_1, J_2) = \frac{\mu}{2}\left[J_1 - 3 + \rho(J_2 - 1)^2\right]. \tag{4.1}$$

Here, μ is the shear modulus encountered in linear elasticity and $\rho \geq 0$ is a material parameter that measures the strength of the fibres, or the degree of anisotropy associated with the employed preferred direction; if $\rho = 0$, then (4.1) reduces to its standard neo-Hookean form, which is associated with isotropic materials.

Using (2.12), (4.1) yields the alternative form

$$\tilde{W}(\gamma, \chi) = \frac{\mu}{2}\left[\chi^2 + \gamma^2 + \chi^{-2} - 3 + \rho(\chi^2 + \gamma^2 - 1)^2\right], \tag{4.2}$$

which yields further

$$\tilde{W}_\gamma = \mu\gamma\left[1 + 2\rho(\chi^2 + \gamma^2 - 1)\right], \qquad \tilde{W}_\chi = \tilde{W}_\gamma\frac{\chi}{\gamma} - \mu\chi^{-3}. \tag{4.3}$$

By virtue of (3.2), (4.3b) leads to

$$\tilde{W}_\chi = \frac{\tau_\theta \hat{b}_1^2}{\gamma r^2} - \mu\chi^{-3}, \tag{4.4}$$

and, since $\gamma = R\hat{g}'(r)$, Eq. (3.5) is converted into

$$\bar{t}_{rr} \equiv \frac{t_{rr}}{\mu} = \int_{\hat{b}_0}^{r}\left(\frac{\bar{\tau}_\theta \hat{b}_1^2}{r^4\hat{g}'(r)}\left[(r\hat{g}'(r))^2 - 1\right] + \frac{r}{r^2 - c}\right)\mathrm{d}r, \qquad \bar{\tau}_\theta = \frac{\tau_\theta}{\mu}. \tag{4.5}$$

The algebraic Eq. (3.6) for the unknown parameter c thus takes the form

$$I(c) \equiv \int_{\hat{b}_0}^{\hat{b}_1}\left(\frac{\bar{\tau}_\theta \hat{b}_1^2}{r^4\hat{g}'(r)}\left[(r\hat{g}'(r))^2 - 1\right] + \frac{r}{r^2 - c}\right)\mathrm{d}r = 0. \tag{4.6}$$

This will be used to determine the unknown parameter c, as soon as the form of $\hat{g}'(r)$ is found.

In this connection, the use of (4.3a) converts (3.2) into the following algebraic equation:

$$\gamma^3 + 3s\gamma - 2q = 0, \tag{4.7}$$

where

$$s = \frac{r^2 - 2c\rho}{6\rho r^2}, \qquad q = \frac{\bar{\tau}_\theta \hat{b}_1^2}{4\rho r\sqrt{r^2 - c}}. \tag{4.8}$$

As already noted in Sect. 3, (4.7) may be alternatively perceived as a first-order ordinary differential equation for the unknown deformation function $\hat{g}'(r)$.

By noting from (3.3) that γ and q are necessarily of the same sign, and then applying to (4.7) Descartes' rule of signs (e.g. [10,11]), one concludes that the latter equation possesses only one positive (negative) real root when

$\bar{\tau}_\theta$ is positive (negative). However, because the fibres are radial, the two different deformations obtained for any pair of opposite $\bar{\tau}_\theta$-values are necessarily mirror images of each other. It is accordingly sufficient to consider only positive values of $\bar{\tau}_\theta$ in what follows and, hence, to seek only the relevant positive root of (4.7); the latter will also provide the form of $\hat{g}'(r)$ through the use of (2.4b).

With $\hat{g}'(r)$ thus becoming known, Eq. (4.6) can be solved for c numerically in the manner outlined at the end of the previous section. The deformation can then be fully determined by evaluating $\hat{g}(r)$ through numerical integration of the obtained single form of $\hat{g}'(r)$. Note that Eqs. (4.6) and (4.7) are interconnected and should therefore be solved simultaneously in every step of the outlined numerical process. As soon as both $\hat{g}(r)$ and c are thereby determined, the distribution of the non-dimensional radial stress component, $\bar{t}_{rr}$, can also be obtained by evaluating numerically the integral shown in Eq. (4.5a). Distributions of the remaining stress components, along with the reaction pressure p, can finally be determined using the constitutive Eqs. (2.13).

5 Limiting case of ideal fibre-reinforced material

In the limiting case in which the fibre strength parameter approaches infinity, the radial fibres involved in the present problem approach their inextensibility limit; the corresponding numerical predictions of the outlined solution should accordingly approach asymptotically their counterparts predicted through a corresponding analysis of an ideal fibre-reinforced material [4,5]. Thus, for numerical comparison purposes, this section refines and, where necessary, extends the part of the relevant solution presented in [4,5], towards complete determination of the stress distributions involved in a tube when its incompressible material is reinforced by inextensible radial fibres.

It is initially noted that the deformation sought was already fully determined in [4,5]. Accordingly, and for positive values of $\bar{\tau}_\theta$, the fibre inextensibility constraint imposes the following relationship between the amount of shear and the radial stretching:

$$\gamma = r g'(R) = \frac{\sqrt{c}}{r} = \sqrt{1-\chi^2}, \tag{5.1}$$

where c is determined in the manner detailed in [4,5]. Note that, although (2.9) still hold, **b** is now necessarily a unit vector along the deformed fibre direction. It is therefore denoted by **a** in this section, thereby leading to

$$a_r = \chi, \qquad a_\theta = \gamma, \qquad a_z = 0. \tag{5.2}$$

Thus, following the analytical process detailed in the appendix, one obtains the in-plane components of the Cauchy stress tensor in the following non-dimensional form:

$$\begin{aligned}
\frac{t_{rr}}{\mu} &= \ln\left(\frac{\sqrt{r^2-c}}{B_0}\right) + \frac{\hat{b}_1^2 \ln(B_1/B_0)}{(B_1-B_0)(B_0B_1-c)}\left(\hat{b}_0^2\frac{\sqrt{r^2-c}}{r^2} - B_0\right),\\
\frac{t_{\theta\theta}}{\mu} &= \ln\left(\frac{\sqrt{r^2-c}}{B_0}\right) + \frac{c\hat{b}_0^2\hat{b}_1^2 \ln(B_1/B_0)}{(B_1-B_0)(B_0B_1-c)}\frac{1}{r^2\sqrt{r^2-c}} + \frac{c}{r^2-c} + \frac{f_1}{\mu},\\
\frac{t_{r\theta}}{\mu} &= \frac{\sqrt{c}\hat{b}_0^2\hat{b}_1^2 \ln(B_1/B_0)}{(B_1-B_0)(B_0B_1-c)}\frac{1}{r^2},
\end{aligned} \tag{5.3}$$

where the value of the constant f_1 is given in (8.27a).

Table 1 Selected numerical predictions of c, $\hat{b}_0$ and $\hat{b}_1$ for different values of non-dimensional external azimuthal traction $\bar{\tau}_\theta$ and fibre strength parameter ρ ($B_0 = 1$ and $B_1 = 3$)

ρ	$\bar{\tau}_\theta$			
	0.1	0.2	0.6	1.3
0.1				
c	−0.154	−0.522	−0.947	−0.981
$\hat{b}_0$	0.92	0.692	0.231	0.137
$\hat{b}_1$	2.974	2.912	2.838	2.832
0.4				
c	−0.042	−0.171	−0.716	−0.909
$\hat{b}_0$	0.979	0.91	0.533	0.302
$\hat{b}_1$	2.993	2.971	2.878	2.844
0.8				
c	0.022	−0.008	−0.409	−0.784
$\hat{b}_0$	1.011	0.996	0.769	0.464
$\hat{b}_1$	3.004	2.999	2.931	2.866
1				
c	0.042	0.041	−0.287	−0.713
$\hat{b}_0$	1.021	1.02	0.844	0.535
$\hat{b}_1$	3.007	3.007	2.952	2.879
2				
c	0.097	0.176	0.099	−0.346
$\hat{b}_0$	1.047	1.084	1.048	0.809
$\hat{b}_1$	3.016	3.029	3.016	2.942
4				
c	0.136	0.277	0.436	0.181
$\hat{b}_0$	1.066	1.13	1.198	1.087
$\hat{b}_1$	3.022	3.046	3.072	3.03
7				
c	0.157	0.333	0.646	0.594
$\hat{b}_0$	1.075	1.155	1.283	1.263
$\hat{b}_1$	3.026	3.055	3.106	3.097
c_{ideal}	0.186	0.429	1.059	1.605

6 Numerical results and discussion

All numerical results presented in this section refer to a tube with undeformed inner and outer radii $B_0 = 1$ and $B_1 = 3$ respectively. Most of the obtained numerical results are presented in graphical form by varying the non-dimensional externally applied azimuthal traction, $\bar{\tau}_\theta$, or the fibre strength parameter, ρ. Numerical values for some of the obtained results are also presented in Table 1 for future comparison purposes.

For different values of the fibre strength parameter ρ, Fig. 2 shows the manner in which the basic deformation parameter c varies with a varying non-dimensional external azimuthal traction $\bar{\tau}_\theta$. It is initially important to note

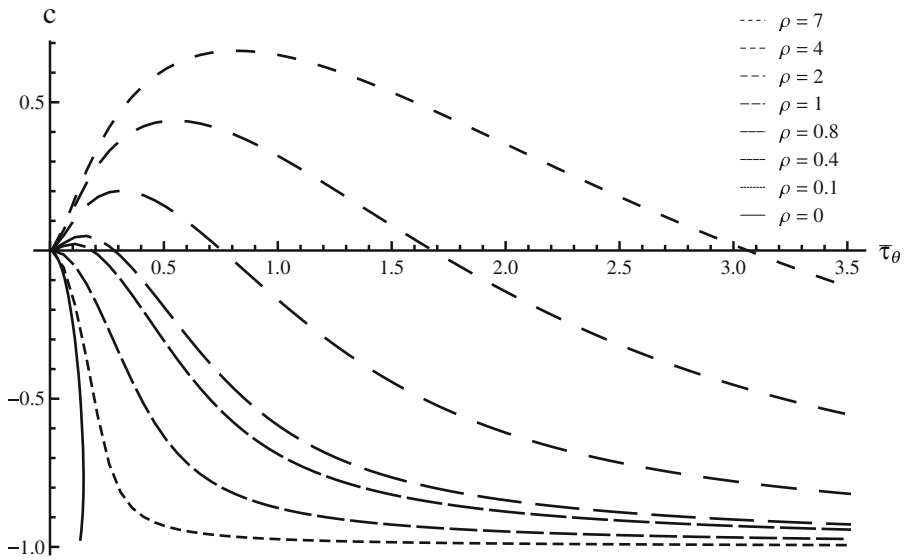

Fig. 2 Variation of c versus $\bar{\tau}_\theta$ for different values of fibre strength parameter ρ

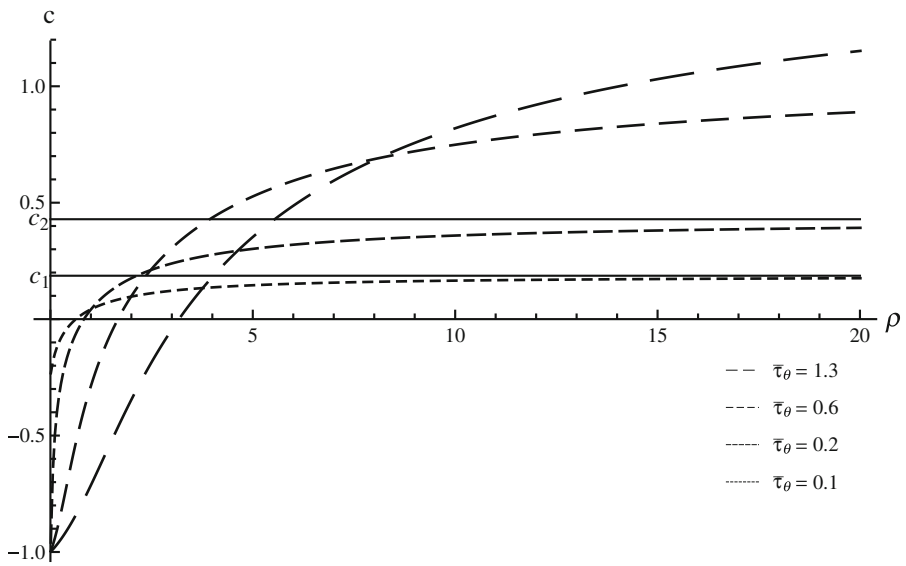

Fig. 3 Variation of c versus ρ for different values of $\bar{\tau}_\theta$

that the case $\rho = 0$ shows the results obtained on the basis of the corresponding isotropic material analysis detailed in [7]. It is important in this connection to recall that c is always negative in the isotropic material case where, as a consequence, both the inner and outer radii of the tube cross section decrease with the deformation. Moreover, the curve denoted by $\rho = 0$ in Fig. 2 attains a maximum of $\bar{\tau}_\theta$ at approximately $(\bar{\tau}_\theta, c) = (0.15, -0.8)$, which is evidently a point of material instability. This is because (1) when the value of $\bar{\tau}_\theta$ approaches that point from below the value of c, and therefore the deformation may jump from one side of the maximum to the other, and (2) the assumed deformation is not attainable for higher values of $\bar{\tau}_\theta$.

However, the slightest non-zero value of ρ stabilises the outlined material behaviour. This becomes evident by observing the curves denoted by $\rho = 0.1$ and $\rho = 0.4$ in Fig. 2, which illustrate the numerical results associated

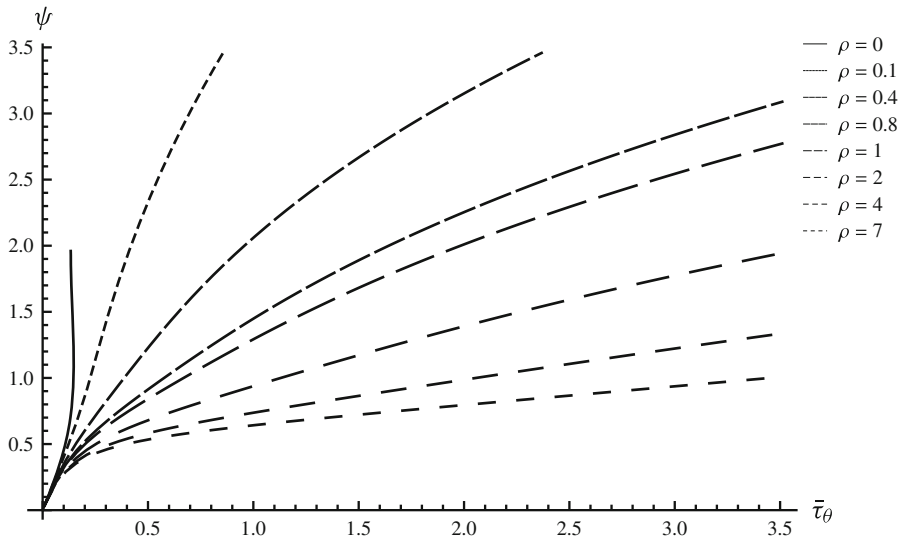

Fig. 4 Variation of ψ versus $\bar{\tau}_\theta$ for different values of ρ

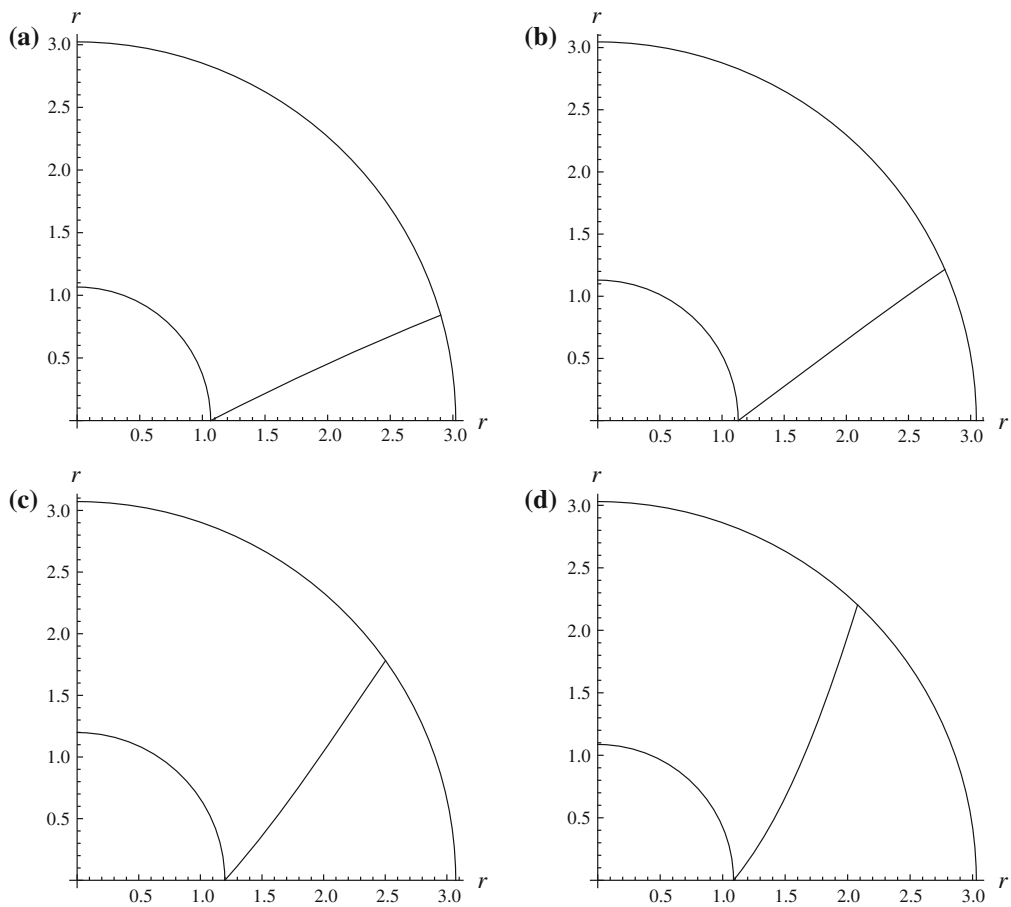

Fig. 5 Deformation pattern of fibre with $\rho = 4$, initially aligned along horizontal radius of tube cross section: **a** $\bar{\tau}_\theta = 0.1$, $c = 0.136$; **b** $\bar{\tau}_\theta = 0.2$, $c = 0.277$; **c** $\bar{\tau}_\theta = 0.6$, $c = 0.436$; **d** $\bar{\tau}_\theta = 1.3$, $c = 0.181$

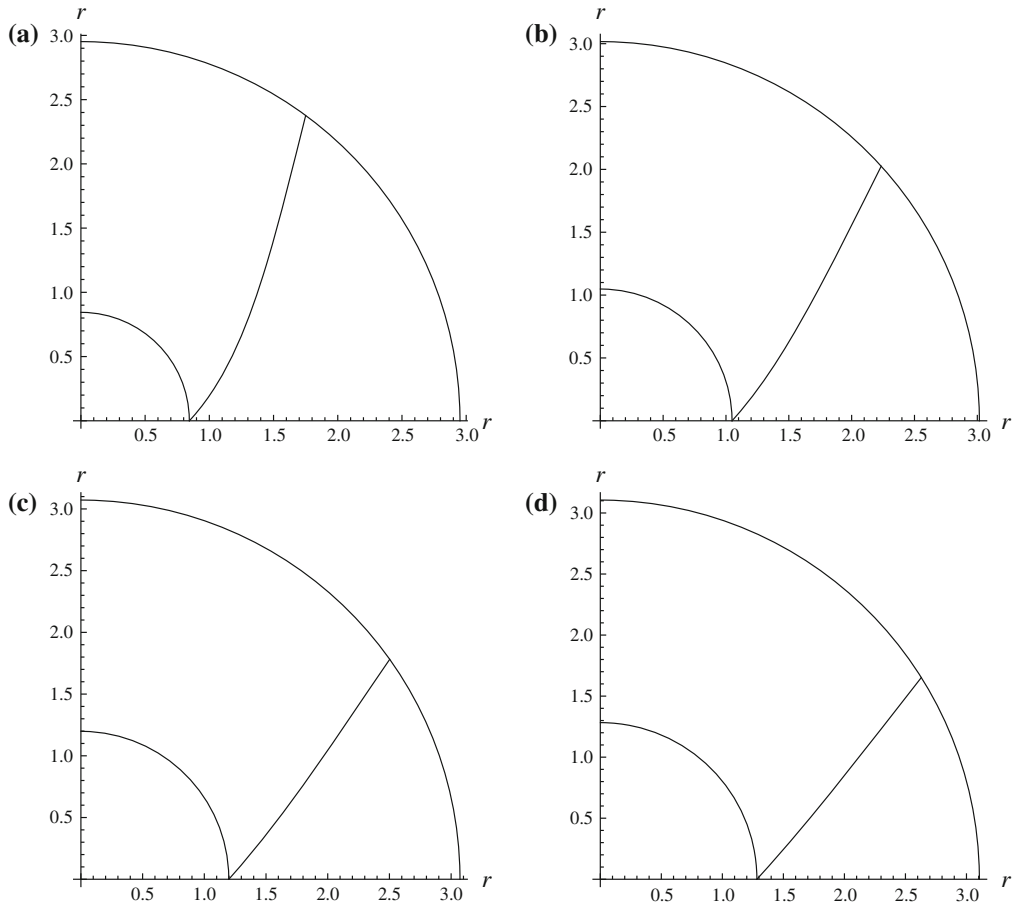

Fig. 6 Deformation pattern of fibre initially aligned along horizontal radius of tube cross section when $\bar{\tau}_\theta = 0.6$: **a** $\rho = 1, c = -0.287$; **b** $\rho = 2, c = 0.098$; **c** $\rho = 4, c = 0.436$; **d** $\rho = 7, c = 0.646$

with tubes reinforced by relatively compliant radial fibres. In either of these cases, the value of c is still always negative, but, unlike the isotropic material case ($\rho = 0$), the assumed deformation is attainable for all positive values of $\bar{\tau}_\theta$. Moreover, either of the depicted curves represents a one-to-one correspondence between $\bar{\tau}_\theta$ and c, while the value of $\bar{\tau}_\theta$ may be increased unboundedly and, hence, approach infinity, thereby allowing the tube to reach asymptotically the limiting geometrical configuration of its non-hollow (solid) counterpart ($c = -B_0^2 = -1$).

On the other hand, when fibres are strong ($\rho > 0.5$), the qualitative relation between corresponding $\bar{\tau}_\theta$- and c-values may generally be divided into three consecutive bands. For relatively small values of $\bar{\tau}_\theta$, c increases monotonically, and as a result, both the inner and outer radii of the tube cross section increase with the deformation. Within this first band of $\bar{\tau}_\theta$-values, which ends when c reaches a positive maximum value, the assumed deformation is influenced predominantly by the strong presence of fibres. However, within the second (middle) band of $\bar{\tau}_\theta$ values, which starts when c begins to decrease monotonically towards zero, the fibres become more compliant to the imposed deformation, while the surrounding matrix material gains influence. The final band of $\bar{\tau}_\theta$ values relates to the observed region of negative c values. There, the tube material resembles the response of its previously discussed counterpart, having embedded compliant fibres; in that case, it is the matrix rather than the fibres which exert a predominant influence on the assumed deformation. The fact that the length of the observed first and second bands of $\bar{\tau}_\theta$ values increases with an increasing fibre strength parameter, ρ, is thus in line with physical expectations.

The outlined observations are reinforced in Fig. 3, where c is plotted against the fibre strength parameter, ρ, for different values of the non-dimensional external azimuthal traction $\bar{\tau}_\theta$. The resemblance of these results to

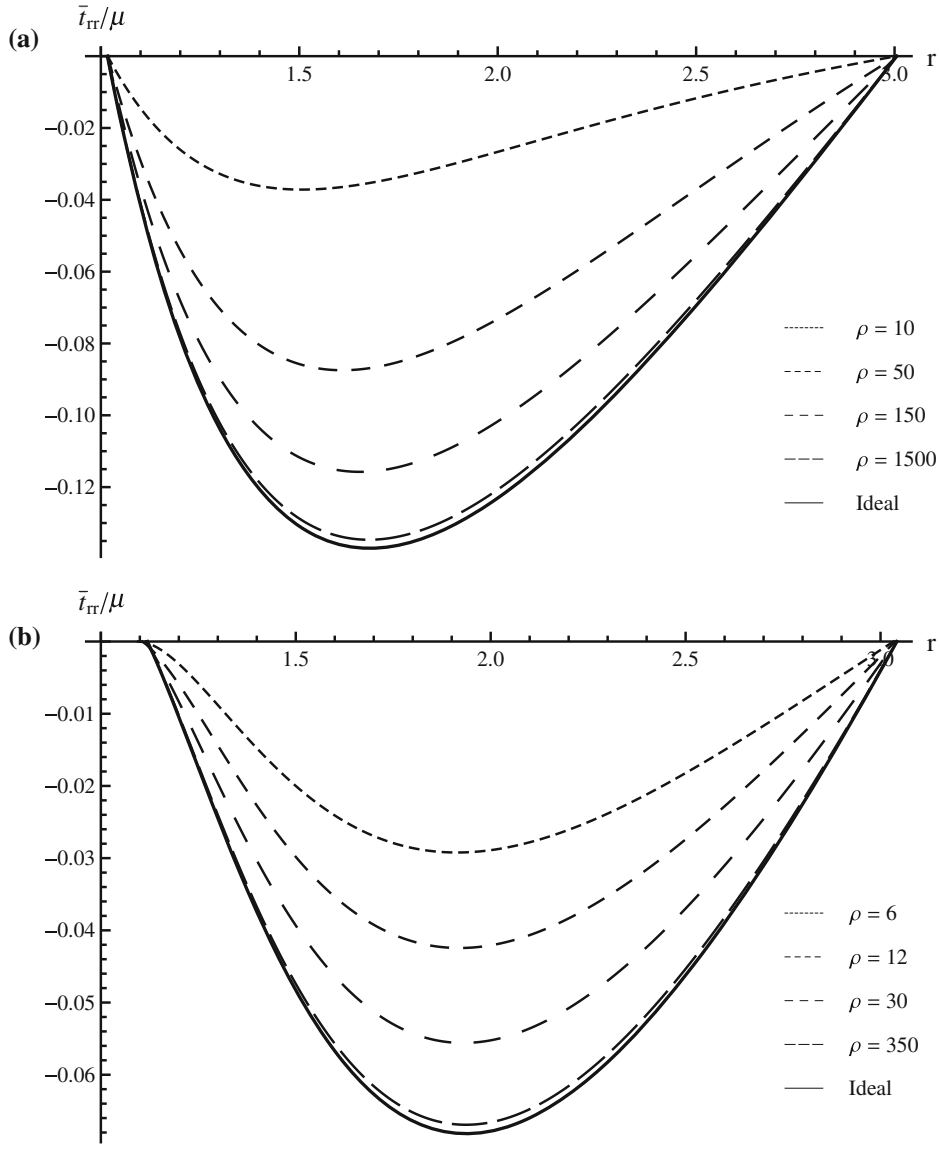

Fig. 7 Non-dimensional radial stress distribution throughout tube cross section for different values of ρ; **a** $\psi = 0.12$ ($\bar{\tau}_\theta = 0.035$), **b** $\psi = 0.3$ ($\bar{\tau}_\theta = 0.126$)

their isotropic material counterparts again becomes clear in this figure, where c is negative for small values of ρ (compliant fibres), while for constant $\bar{\tau}_\theta$ it turns positive at larger values of ρ (strong fibres). Figure 3 shows further that, regardless of the value of $\bar{\tau}_\theta$, c increases monotonically with increasing ρ and, at the limit, approaches asymptotically the value it obtains in the corresponding ideal fibre-reinforced material case (Sect. 5), where fibres are assumed to be inextensible. That limiting value is marked in Fig. 3 by the depicted horizontal asymptotes which emanate from $c = c_1$ when $\bar{\tau}_\theta = 0.1$ and $c = c_2$ when $\bar{\tau}_\theta = 0.2$.

The depicted limiting values of c (Fig. 3) are obtained by applying the boundary condition (2.18c) on Eq. (5.3c), leading to the following algebraic equation:

$$\bar{\tau}_\theta = \frac{\sqrt{c}(B_0^2 + c)}{(B_1 - B_0)(B_0 B_1 - c)} \ln\left(\frac{B_1}{B_0}\right). \tag{6.1}$$

This equation was solved numerically for the values of $\bar{\tau}_\theta$ presented in Table 1 to yield the corresponding values of c denoted there by c_{ideal}. Figure 3 finally makes clear that the smaller the value of $\bar{\tau}_\theta$, the faster c leaves its negative-value region and approaches the value it attains in its ideal fibre-reinforced material limit.

For the values of the fibre strength parameter ρ employed in Fig. 2, Fig. 4 depicts the manner in which the azimuthal angle ψ predicted on the outer boundary varies with a varying the externally applied azimuthal traction $\bar{\tau}_\theta$. The curve which represents the isotropic material case ($\rho = 0$) shows again the material instability feature observed in Fig. 2 near $\bar{\tau}_\theta = 0.15$. However, that feature is again absent for non-zero values of ρ. The figure shows further that for small values of $\bar{\tau}_\theta$ ($\bar{\tau}_\theta < 0.1$) the value of the fibre strength parameter, ρ, leaves essentially unaffected the nearly linear relationship observed between $\bar{\tau}_\theta$ and ψ. However, as the value of $\bar{\tau}_\theta$ is increased, this relationship becomes highly non-linear as well as highly dependent on the value of ρ. Thus, for non-zero values of ρ, the value of ψ increases monotonically as $\bar{\tau}_\theta$ increases and, in agreement with physical expectations, decreases as the fibre strength parameter, ρ, increases, for fixed $\bar{\tau}_\theta$ values.

Figures 5 and 6 focus on the first quadrant of the deformed tube cross section and, for different values of $\bar{\tau}_\theta$ and ρ, respectively, depict the deformation pattern of a fibre initially aligned along the horizontal radius; in Fig. 5, the fibre strength parameter is fixed at $\rho = 4$, while Fig. 6 keeps fixed the value of $\bar{\tau}_\theta$ ($= 0.6$). In agreement with physical expectations, the azimuthal angle increases throughout the tube cross section with an increasing $\bar{\tau}_\theta$ (Fig. 5), while it decreases with an increasing fibre strength parameter (Fig. 6).

For two different values of the externally applied azimuthal angle ψ (or, alternatively, traction $\bar{\tau}_\theta$) and for different values of the fibre strength parameter ρ, Fig. 7 illustrates the predicted distribution of the non-dimensional radial stress $\bar{t}_{rr}$ throughout the tube cross section. It is seen that the absolute value of radial stresses increases with increasing ρ, while for large ρ values, their distribution closely approaches its ideal fibre-reinforced material counterpart; the latter is marked by a solid line and also noted as *ideal* in the figure. The fact that the curve approaches its ideal fibre-reinforced material limit in an essentially asymptotic manner is verified numerically, in the sense that any further increase in ρ beyond the highest value shown in the figure leaves practically unaffected the form of the depicted curve.

7 Conclusions

In physical terms, the hyper-elasticity problem considered in this paper is an intermediate step between the problem of the area-preserving azimuthal shear deformation of a circular cylindrical tube made of incompressible isotropic material [7] and that of a tube made of incompressible material with embedded inextensible straight fibres, aligned initially along the radial direction of its undeformed cross section [4,5].

The fibre-inextensibility constraint imposed in [4,5] simplified the formulation of the present plane-strain problem to such an extent that the corresponding solution is essentially based on completely analytical means (see also the appendix). Similarly, the mathematical difficulty of the problem is reduced considerably in the case of material isotropy [7], where, as a result, only a certain part of the corresponding solution requires direct numerical treatment. In contrast, the advanced degree of mathematical difficulty involved in the formulation of the present problem, where the material is transversely isotropic but the embedded straight fibres are extensible, requires numerical treatment for a substantial part of the outlined solution.

Nevertheless, the presented numerical results are indeed in line with the fact that the present problem, as well as its solution, reflects a physical situation which is between the simpler relevant cases considered and studied separately in [7] and [4,5]. It is seen in this context that both the inner and outer radii of the tube cross section decrease with the assumed deformation if the fibres are very compliant, precisely as happens in the case of material isotropy [7], where the tube thickness increases with the deformation.

In contrast, strong fibres resist the applied azimuthal shear deformation in a manner analogous to that observed in [4,5], where the fibres were assumed to be inextensible. Accordingly, if the imposed deformation is relatively small, then strong extensible fibres resist considerably any change in their straight initial shape, thereby forcing a decrease in the tube's thickness by increasing both its inner and outer radii. However, such fibres become more

compliant to intermediate amounts of azimuthal shear strain where, despite the notable change in their initial straight shape, they are still able to increase the inner and outer radii of the tube and, hence, decrease its thickness. Finally, there is always a region of relatively high amounts of azimuthal shear strain where, regardless of their strength, extensible fibres become compliant to the imposed deformation. Both the inner and outer radii of the tube cross section decrease in that region in which the thickness of the deformed tube is thus increased.

These observations are supported by relevant numerical comparisons which illustrate the manner in which fibre strength or the amount of azimuthal shear strain affects the stress distributions developed throughout the tube thickness. Accordingly, the absolute value of radial normal stresses increases with an increasing amount of applied azimuthal shear strain or fibre strength. It is thus instructive to note that when the fibre strength is increased substantially, the distribution of radial normal stress predicted throughout the tube cross section approaches asymptotically the corresponding distribution predicted by the simpler and entirely different mathematical analysis outlined in [4,5] on the basis of the ideal fibre-reinforced material concept.

Appendix: Inextensible fibres

Using the components of **a** defined in (5.2), the equation of the deformed fibres (the so-called a-curves) is found to be

$$\theta - \Theta = \int \frac{a_\theta}{r a_r} \mathrm{d}r = \sec^{-1}\left(\frac{r}{\sqrt{c}}\right) - \sec^{-1}\left(\frac{\hat{b}_0}{\sqrt{c}}\right). \tag{8.1}$$

The orthogonal trajectories of the a-curves in the plane of the deformed cross section define the so-called n-curves [6], having unit tangent

$$\mathbf{n} = (n_r, n_\theta, 0)^{\mathrm{T}} = (a_\theta, -a_r, 0)^{\mathrm{T}} = (\gamma, -\chi, 0)^{\mathrm{T}}. \tag{8.2}$$

The equation of those curves is therefore

$$\theta - \Theta = \int \frac{n_\theta}{r n_r} \mathrm{d}r = \left(\frac{r^2}{c} - 1\right)^{1/2} - \sec^{-1}\left(\frac{r}{\sqrt{c}}\right) - \left(\frac{\hat{b}_0^2}{c} - 1\right)^{1/2} + \sec^{-1}\left(\frac{\hat{b}_0}{\sqrt{c}}\right). \tag{8.3}$$

These two families of curves define a local, orthogonal, curvilinear co-ordinate system, which will be found useful when equilibrium is considered.

Due to the plane-strain nature of the problem, the constraints of material incompressibility and fibre inextensibility leave independent only one of the invariants (2.12) [6]. This may be chosen to be J_1, and the strain energy density should be regarded a general function of it, namely

$$W = W(J_1). \tag{8.4}$$

The corresponding constitutive equations can then be deduced directly from [4] by neglecting the fibre bending stiffness terms considered there.

Hence, considering that the implied inextensible fibres are perfectly flexible, one obtains

$$\begin{aligned} &t_{\alpha\beta} = -p\delta_{\alpha\beta} + T a_\alpha a_\beta + s_{\alpha\beta}, \quad t_{zz} = -p, \\ &s_{\alpha\beta} = 2W_1 B_{\alpha\beta} - 2W_1 \delta_{\alpha\beta} - 2(J_1 - 3) W_1 a_\alpha a_\beta, \\ &s_{zz} = 0, \end{aligned} \tag{8.5}$$

where T is the arbitrary tension that represents the reaction of the material to the constraint of fibre inextensibility. Moreover, $s_{\alpha\beta}$ are the components of the so-called extra stress tensor (with the exception of r, θ and z, as well as a and n below, Latin indices operate in three dimensions, Greek indices in two dimensions). In addition, consistency with the imposed material constraints requires that the components of the extra stress tensor satisfy the following conditions [4,6]:

$$s_{ii} = 0, \qquad s_{ij} a_i a_j = 0, \tag{8.6}$$

where repeated indices imply summation over the range of their values.

In the aforementioned local curvilinear co-ordinate system, the components of the extra stress tensor are described as follows [4,6,12]:

$$s_{\alpha\beta} = s_a a_\alpha a_\beta + s_n n_\alpha n_\beta + \tau(a_\alpha n_\beta + a_\beta n_\alpha), \tag{8.7}$$

where s_a and s_n are the normal components of the extra stress tensor, and hence

$$\tau = s_{\alpha\beta} a_\alpha n_\beta \tag{8.8}$$

represents the local shear stress component. Thus, when the constraint Eqs. (8.6) are combined with (8.5d), (8.7) reduces to

$$s_{\alpha\beta} = \tau(a_\alpha n_\beta + a_\beta n_\alpha), \tag{8.9}$$

in which τ is to be determined using constitutive equations as soon as the form of the strain energy density of the material becomes available.

For consistency with the application detailed in Sect. 4, it is now assumed that the strain energy density is that of the standard neo-Hookean material, namely

$$W(J_1) = \frac{\mu}{2}(J_1 - 3), \qquad W_1 = \frac{\partial W}{\partial J_1} = \frac{\mu}{2}, \tag{8.10}$$

where, after (2.12a) and (5.1), J_1 necessarily takes the form

$$J_1 = \mathrm{tr}(\mathbf{B}) = \chi^{-2} + 2. \tag{8.11}$$

The constitutive Eq. (8.5c) then yields the non-zero components of the extra stress tensor as follows:

$$s_{rr} = 2\mu(\chi^2 - 1) = -\frac{2\mu c}{r^2}, \quad s_{\theta\theta} = 2\mu\gamma^2 = \frac{2\mu c}{r^2}, \quad s_{r\theta} = \mu\chi\gamma(2 - \chi^{-2}) = \frac{\sqrt{c}(r^2 - 2c)}{r^2\sqrt{r^2 - c}}, \tag{8.12}$$

and hence (8.8) leads to

$$\tau = -\frac{\mu\gamma}{\chi} = -\frac{\mu\sqrt{c}}{\sqrt{r^2 - c}}. \tag{8.13}$$

Equations (8.5) thus reveal that the only remaining stress unknowns are the functions p and T, which must be determined by solving the two simultaneous equations of static equilibrium.

Those equilibrium equations obtain a standard form in the local co-ordinate system of the a- and n-curves [4,6,12], which, in the absence of body forces, is as follows:

$$\frac{\partial t_a}{\partial l_a} + \kappa_n(t_a - t_n) = 2\kappa_a\tau - \frac{\partial \tau}{\partial l_n}, \quad \frac{\partial t_n}{\partial l_n} + \kappa_a(t_a - t_n) = -2\kappa_n\tau - \frac{\partial \tau}{\partial l_a}. \tag{8.14}$$

Here, p and T are replaced by the new pair of unknowns

$$t_a = -p + T, \qquad t_n = -p, \tag{8.15}$$

and therefore the in-plane Cauchy stress components (8.5a) take the following alternative form:

$$t_{\alpha\beta} = t_a a_\alpha a_\beta + t_n n_\alpha n_\beta + \tau(a_\alpha n_\beta + a_\beta n_\alpha). \tag{8.16}$$

In (8.14), l_a and l_n denote the arc length along the a- and n-curves respectively, while κ_a and κ_n are the curvatures of those curves defined as follows:

$$\kappa_a = -\nabla \cdot \mathbf{n}, \qquad \kappa_n = \nabla \cdot \mathbf{a}. \tag{8.17}$$

Thus, using (5.2) and (8.2), it is seen that

$$\kappa_a = 0, \qquad \kappa_n = R^{-1} = \frac{1}{\sqrt{r^2 - c}}, \tag{8.18}$$

making it immediately clear that the fibres remain straight and, in accordance with theoretical expectations [6], the n-curves maintain their curvature after deformation. Moreover, the use of (8.1) and (8.3) provides the necessary relationship between the deformed cylindrical polar co-ordinates and the co-ordinates of the curvilinear local co-ordinate system; this is as follows:

$$\mathrm{d}l_a = \frac{r}{\sqrt{r^2 - c}}\mathrm{d}r = \mathrm{d}R, \qquad \mathrm{d}l_n = \frac{r}{\sqrt{c}}\mathrm{d}r. \tag{8.19}$$

Using these results, the equilibrium equations (8.14) reduce to

$$\frac{\partial t_a}{\partial l_a} + l_a^{-1}t_a = l_a^{-1}t_n - \frac{\partial \tau}{\partial l_n}, \qquad \frac{\partial t_n}{\partial l_n} = -\frac{2\tau}{\sqrt{r^2 - c}} - \frac{\partial \tau}{\partial l_a}. \tag{8.20}$$

Equation (8.20b) can be integrated immediately along the n-curves to give

$$t_n = -\int_{\hat{b}_0}^{r} \left[\frac{-2\mu\sqrt{c}}{r^2 - c} + \mu\sqrt{c}r(r^2 - c)^{-3/2}\frac{\sqrt{r^2 - c}}{r}\right]\frac{r}{\sqrt{c}}\mathrm{d}r + f_1(l_a) = \mu \ln\left(\frac{\sqrt{r^2 - c}}{B_0}\right) + f_1(l_a), \tag{8.21}$$

where $f_1(l_a)$ is an arbitrary function of integration. Equation (8.20a) can also be integrated subsequently along the a-curves to yield

$$t_a = l_a^{-1}\int_{\hat{b}_0}^{r}\left(t_n - l_a\frac{\partial \tau}{\partial l_n}\right)\frac{\mathrm{d}l_a}{\mathrm{d}r}\mathrm{d}r + f_2(l_n), \tag{8.22}$$

where $f_2(l_n)$ is a second arbitrary function of integration.

Use of the boundary conditions (2.17a) and (2.18a) in connection with (8.16) yields the pair of algebraic equations [4,5]

$$t_a\Big|_{r=\hat{b}_k} + \frac{c}{B_k^2} t_n\Big|_{r=\hat{b}_k} = -\frac{2\sqrt{c}}{B_k}\tau\Big|_{r=\hat{b}_k} \qquad (k=0,1), \tag{8.23}$$

which are used in connection with (8.21b) and (8.22) to determine the arbitrary functions $f_1(l_a)$ and $f_2(l_n)$. Application of the first of these boundary conditions ($k=0$) yields

$$f_2(l_n) + \frac{c}{B_0^2} f_1(l_a) = \frac{2\mu c}{B_0^2}. \tag{8.24}$$

Since l_a and l_n are independent variables, (8.24) can be satisfied only if $f_1(l_a)$ and $f_2(l_n)$ are both constant; these constants are denoted in what follows by f_1 and f_2 respectively.

Application of the boundary condition (8.23) at the outer tube boundary ($k=1$) further yields

$$f_2 + \frac{c}{B_1^2} f_1 = \frac{2\mu c}{B_1^2} - \frac{\mu c}{B_1^2} \ln\left(\frac{B_1}{B_0}\right) - \frac{M}{B_1}, \tag{8.25}$$

where the constant M is given as follows:

$$M = \int_{\hat{b}_0}^{\hat{b}_1} \left(t_n - l_a \frac{\partial \tau}{\partial r}\frac{\partial r}{\partial l_n}\right)\frac{\mathrm{d}l_a}{\mathrm{d}r}\mathrm{d}r = (B_1 - B_0)\left[f_1 - \mu\left(1 + \frac{c}{B_0 B_1}\right)\right] + \mu B_1 \ln\left(\frac{B_1}{B_0}\right). \tag{8.26}$$

Solving (8.24) and (8.25) simultaneously, we obtain the values of f_1 and f_2 as

$$f_1 = \mu - \frac{\mu B_0 \hat{b}_1^2}{(B_1 - B_0)(B_0 B_1 - c)} \ln\left(\frac{B_1}{B_0}\right), \quad f_2 = \frac{\mu c}{B_0} + \frac{\mu c \hat{b}_1^2}{(B_1 - B_0)(B_0 B_1 - c)} \ln\left(\frac{B_1}{B_0}\right). \tag{8.27}$$

Hence, performing the integration presented in (8.22), one finds

$$t_a = \mu \ln\left(\frac{\sqrt{r^2 - c}}{B_0}\right) + \frac{\mu c}{r^2 - c} + \frac{\mu \hat{b}_0^2 \hat{b}_1^2 \ln(B_1/B_0)}{(B_1 - B_0)(B_0 B_1 - c)} \frac{1}{\sqrt{r^2 - c}} + f_1 - \mu. \tag{8.28}$$

With t_a and t_n now known, the unknown functions p and T can also be determined; using (8.15), we find them to be

$$p(r) = -\mu \ln\left(\frac{\sqrt{r^2 - c}}{B_0}\right) - f_1, \quad T(r) = \frac{\mu c}{r^2 - c} + \frac{\mu \hat{b}_0^2 \hat{b}_1^2 \ln(B_1/B_0)}{(B_1 - B_0)(B_0 B_1 - c)} \frac{1}{\sqrt{r^2 - c}} - \mu. \tag{8.29}$$

Thus, the components of the Cauchy stress tensor can be deduced from the constitutive Eqs. (8.5), which lead to their final explicit form (5.3).

References

1. Rivlin RS (1949) Large elastic deformations of isotropic materials. VI. Further results in the theory of torsion, shear and flexure. Philos Trans R Soc Lond Ser A Math Phys Sci 242(845):173

2. Kassianidis F, Ogden RW, Merodio J, Pence TJ (2008) Azimuthal shear of a transversely isotropic elastic solid. Math Mech Solids 13(8):690
3. Dorfmann A, Merodio J, Ogden RW (2010) Non-smooth solutions in the azimuthal shear of an anisotropic nonlinearly elastic material. J Eng Math 68(1):27–36
4. Soldatos KP (2010) Second-gradient plane deformations of ideal fibre-reinforced materials: implications of hyper-elasticity theory. J Eng Math 68(1):99–127
5. Soldatos KP (2009) Azimuthal shear deformation of an ideal fibre-reinforced tube according to a second gradient hyper-elasticity theory. In: Proceedings of the 7th EUROMECH solid mechanics conference. Portugal, Lisbon, September, pp 7–11
6. Spencer AJM (1972) Deformations of fibre-reinforced materials. Oxford University Press, London
7. Dagher MA, Soldatos KP (2013) Area-preserving azimuthal shear deformation of an incompressible isotropic hyper-elastic tube. J Eng Math 78(1):131–142
8. Qiu GY, Pence TJ (1997) Loss of ellipticity in plane deformation of a simple directionally reinforced incompressible nonlinearly elastic solid. J Elast 49(1):31–63
9. Merodio J, Ogden RW (2002) Material instabilities in fiber-reinforced nonlinearly elastic solids under plane deformation. Arch Mech 54(5):525–552
10. Hart WL (1966) College Algebra, 5th edn. D. C. Heath and Company, Lexington, Massachusetts
11. Griffiths LW (1947) Introduction to the theory of equations. Wiley, New York
12. Pipkin AC, Rogers TG (1971) Plane deformations of incompressible fiber-reinforced materials. J Appl Mech 38:634–640